

## Scaling of the Interface Roughness in Fe-Cr Superlattices: Self-Affine versus Non-Self-Affine

J. Santamaria,<sup>1,\*</sup> M. E. Gómez,<sup>1,†</sup> J. L. Vicent,<sup>2</sup> K. M. Krishnan,<sup>3</sup> and Ivan K. Schuller<sup>1</sup>

<sup>1</sup>*Department of Physics, University of California–San Diego, La Jolla, California 92093-0319*

<sup>2</sup>*Departamento de Física de Materiales, Universidad Complutense, 28040 Madrid, Spain*

<sup>3</sup>*Department of Materials Sciences, University of Washington, Seattle, Washington 98195-2120*

(Received 15 April 2002; published 16 October 2002)

We have analyzed kinetic roughening in Fe-Cr superlattices by energy-filtered transmission electron microscopy. The direct access to individual interfaces provides both static and dynamic roughness exponents. We find an anomalous non-self-affine scaling of the interface roughness with a time dependent local roughness at short length scales. While the deposition conditions affect strongly the long-range dynamics, the anomalous short-range exponent remains unchanged. The different short- and long-range dynamics outline the importance of long-range interactions in kinetic roughening.

DOI: 10.1103/PhysRevLett.89.190601

PACS numbers: 68.55.Jk, 05.40.-a, 81.10.Aj, 81.15.Cd

The analysis of surface morphology of thin films is a subject of intense activity. Despite the complexity of the growth process, theoretical and experimental studies have shown that kinetic roughening frequently obeys relatively simple scaling laws (*self-affine* roughness) [1]. In superlattices, with many (buried) interfaces, the evolution of roughness is considerably more complicated and remains unexplored. Unfortunately, determining quantitatively the interface structure from diffuse x-ray scattering [2–5] requires assumptions on the nature of the roughness (assumed generally *self-affine* [6]) and the existence of a single lateral correlation length for the various interfaces. However, a direct proof of these assumptions is lacking. Here by imaging directly the interfaces we determine simultaneously static and dynamic critical exponents. We provide evidence for *non-self-affine* anomalous roughness in superlattices with a power law dependent local interfacial slope.

A rough surface can be characterized by fluctuations of surface height around its mean value,  $z(x, t) = h(x, t) - \langle h(x, t) \rangle$ , at a position  $x$  and a time  $t$ . The local surface width is defined as  $\sigma(l, t) = [\langle z^2(x, t) \rangle]^{1/2}$ , where the brackets denote an average over a lateral length scale,  $l$ , in a system of size  $L$  ( $l < L$ ). Alternatively, roughness correlations over a distance  $l$  can be obtained from the height-height correlation function  $g(l, t) = \langle [h(x+l, t) - h(x, t)]^2 \rangle^{1/2}$ . Both pictures are equivalent since numerical simulations show  $g(l, t) \propto \sigma(l, t)$  [1]. For many surfaces, the surface width scales according to the Family-Vicsek [7] scaling ansatz,

$$\sigma(l, t) = t^\beta f(l/t^{1/z}), \quad (1)$$

where the scaling function  $f(u)$  behaves as  $u^\alpha$  if  $u \ll 1$  and is constant for  $u \gg 1$ . The local surface width thus increases as  $\sigma(l, t) \propto l^\alpha$  until it saturates at a value  $\sigma_s(t)$ , for  $l$  larger than an in-plane cutoff length,  $\xi$ , the lateral roughness correlation length. The saturation surface width and lateral roughness correlation length grow

with time (thickness) following power laws with different dynamic exponents,  $\sigma_s(t) \propto t^\beta$  and  $\xi(t) \propto t^{1/z}$ , and the relation  $z = \alpha/\beta$  holds [1]. In *self-affine* surfaces, local  $[\sigma(l, t) \propto l^\alpha]$  and global  $[\sigma(L, t) = L^\alpha]$  interface width scale with the same roughness exponent  $\alpha$  [1], and for short length scales  $\sigma(l, t)$  is independent of deposition time.

Recently, growth models [8–10] with different roughness exponents at short ( $\alpha_{\text{loc}}$ ) and long ( $\alpha$ ) length scales have been proposed which correspond to a *non-self-affine* scaling ansatz [11,12]. The local interface width is no longer time independent at short distances; it follows a power law with a new exponent  $\beta_{\text{loc}}$ , while at long lengths it scales as  $t^\beta$ . The lateral roughness correlation length still scales as  $\xi(t) \propto t^{1/z}$ , but the exponents obey  $\alpha_{\text{loc}} = \alpha - \beta_{\text{loc}}z$  and  $\alpha_{\text{loc}} = (\beta - \beta_{\text{loc}})z$  [11]. A nonstationary local interface width of the form  $\sigma(l, t) = l^\alpha \sqrt{\ln(t)}$  used in models incorporating surface diffusion [13,14] was observed in thin films with a linear diffusion limited growth [15,16]. However, the power law dependence of the local interface width at short length scales has been observed only very recently in Cu [17] and in polymer thin films [18].

For superlattices the interfacial width and in-plane correlation length may increase from layer to layer, although their evolution is not clear *a priori*, due to the presence of more than one constituent. In other words, the extension of scaling concepts from single surfaces to superlattices is not straightforward. So far, interface characterization used mainly diffuse x-ray reflectivity (XRR), which provides averaged information over all interfaces. Extracting *quantitative* information relies on assumptions concerning the nature of the roughness; i.e., (a) the individual interfaces are *self-affine* and (b) a single correlation length is assumed for all interfaces (correlated roughness). X-ray spectra are simulated using a single height-height correlation function assuming  $\langle [h_n(x+l, t) - h_n(x, t)]^2 \rangle = 2\sigma^2\{1 - \exp[-(l/\xi)^{2\alpha}]\}$  which implies a single (averaged) roughness cutoff

length [2–6]. The validity of these assumptions in superlattices has not been checked with techniques probing individual layers.

Here we address this problem in sputtered Fe-Cr superlattices using chemically sensitive imaging by transmission electron microscopy on cross-section samples. Special care was taken to ensure that the measurements are free of errors due to projection or multiple scattering effects [19]. Composition profiles of the *individual layers* were statistically analyzed to extract the interface width and its lateral correlation length. The roughness scaling behavior was examined for two types of samples: those grown at low-pressure exhibiting columnar structure and those at high-pressure in which the growth is dominated by diffusive transport and thermalization in the sputtering gas.

[Fe(3 nm)/Cr(1.2 nm)]<sub>20</sub> superlattices were grown by dc sputtering sandwiched between 100 nm Nb thick buffer and capping layers. The growth pressure was varied between 4 and 10 mTorr. The Nb layers were always grown at an Ar pressure of 3 mTorr and with the same thickness, to ensure that the Nb-buffer layer always had the same roughness. A detailed description of the growth and transport measurements has been reported elsewhere [19].

Electron microscopy was carried out using a Philips CM20-FEG TEM equipped with a Gatan Imaging Filter, capable of obtaining both electron energy-loss spectra and energy-filtered images in real time at high spatial resolution. Cross-section TEM samples were prepared following customary polishing, dimpling, and low angle (< 10°) ion milling to get large electron transparent regions thin enough for electron energy loss spectral investigations without multiple scattering. Energy-filtered imaging techniques (EFTEM) (after removal of the background due to other loss processes) on cross-sectional samples provide Fe or Cr elemental maps at sufficient resolution to quantify the local structural roughness at the Fe-Cr or Cr-Fe interfaces. Two different methods (“three windows” or “jump ratio”) were used to account for the uncharacteristic background [19].

A possible problem with this technique is that the 2D roughness is projected along the cross-section thickness into a one-dimensional (1 + 1) profile. However, the roughness and the inelastic or multiple scattering mean free path are comparable or larger than the cross-section thickness [20]. Thus our conclusions are free from projection artifacts.

Typical cross-section EFTEM maps of sputtered [Fe(3 nm)/Cr(1.2 nm)]<sub>n</sub> superlattices are shown in Figs. 1(a) and 1(c). The bright intensity is proportional to the intensity of the Fe-characteristic L<sub>2,3</sub> energy-loss signal; dark regions mean absence of Fe. EFTEM maps (150–200 nm wide) were digitized with the Gatan-Digital-Micrograph software integrating the intensity over windows 2.7 nm wide centered around points sepa-

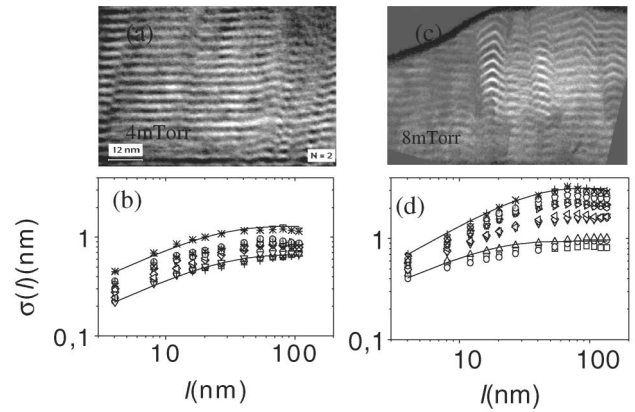


FIG. 1. Energy filtered Fe L<sub>2,3</sub> maps of [Fe(3 nm)/Cr(1.2 nm)]<sub>20</sub> superlattices grown (a) at 4 mTorr and (b) at 8 mTorr. Lateral evolution of the local interface width  $\sigma(l)$  for the different bilayers for samples grown (c) at 4 mTorr and (d) at 8 mTorr. Different data sets correspond to different bilayer indexes (1 to 20). Lines in the figure are fits to  $\sigma_n(l) = \sigma_{s,n}\{1 - \exp[-(l/\xi_{\parallel})^{2\alpha}]\}^{1/2}$ . Note that  $l < L$  and  $\xi_{\parallel} \ll L$  always.

rated 1.35 nm (5 pixels) [21]. The maximum intensity locii for each bilayer define the bilayer profile. The fluctuations in the interface heights were statistically analyzed for the different bilayers.

Interestingly, for the individual layers  $h_n(x + l, t) - h_n(x, t)$  has a Gaussian distribution with a standard deviation  $\langle [h_n(x + l, t) - h_n(x, t)]^2 \rangle^{1/2}$  increasing with distance  $l$  between points [6]. Thus, our results provide a direct proof of the random Gaussian distribution of height differences for the individual bilayers. This is a central assumption in many quantitative interpretation of diffuse XRR [2–6, 20, 22]. This was verified for all samples. The local interface width  $\sigma(l, t) = [\langle z^2(x, t) \rangle]^{1/2}$  was analyzed for individual bilayers using the standard deviation of the distribution of heights  $z_n(x, t) = h_n(x, t) - \langle h_n(x, t) \rangle$  for each bilayer. Note that averages are done over a window width  $\ell$  around each point. Figure 1 shows  $\sigma(l, t)$  vs the window width for the individual bilayers, for samples with  $N = 20$  bilayers grown at 8 mTorr 1(b) and 5 mTorr 1(d). Interestingly, in distinction of *self-affine* surfaces, the interface width  $\sigma(l, t)$  depends on thickness (time) at small length scales [Figs. 1(b) and 1(d)]. Moreover, the data sets for the low-pressure sample [Figs. 1(a) and 1(c)] shift nearly parallel to each other as the bilayer index (time) changes. This indicates that kinetic roughening cannot be described by a Family-Vicsek scaling ansatz, Eq. (1), and that anomalous scaling of Eq. (1) may apply (*non-self-affine* interfaces).

The roughness increases with lateral window size  $l$  according to a power law  $\sigma(l) \propto l^{\alpha_{loc}}$  and then saturates. The position of the “knee” at saturation is a measure of the lateral correlation length  $\xi_{\parallel}$  of the roughness.  $\xi_{\parallel}$  is extracted from fits [lines in Figs. 1(b) and 1(d)] of the roughness for each bilayer to the expression  $\sigma_n(l) = \sigma_{s,n}\{1 - \exp[-(l/\xi_{\parallel})^{2\alpha_{loc}}]\}^{1/2}$ , where  $\sigma_{s,n}$  is the saturation

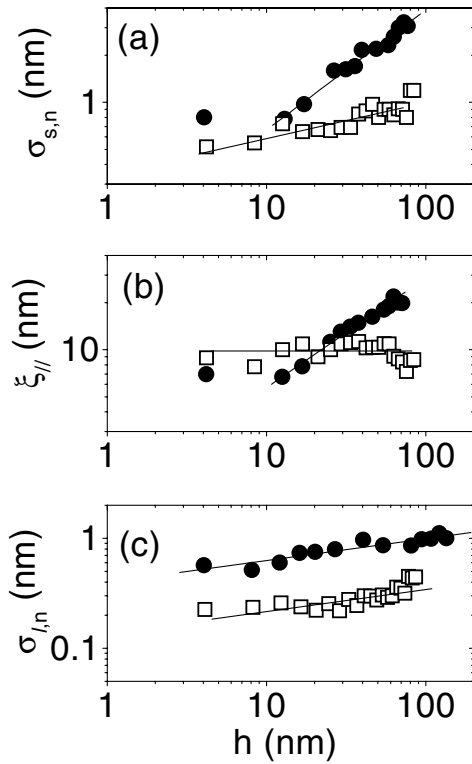


FIG. 2. Thickness (time) dependence of the following: (a) saturation interface width, (b) roughness lateral correlation length, and (c) short-range local interface width for low (4 mTorr, open squares) and high (8 mTorr, solid circles) pressure samples.

value of the roughness for bilayer  $n$ , and  $\alpha_{\text{loc}}$  is the roughness exponent [6]. Thus, the asymptotic behavior  $\sigma_n(l \ll \xi_{\parallel}) \approx l^{\alpha_{\text{loc}}}$  and  $\sigma_n(l \gg \xi_{\parallel}) \approx \sigma_{s,n}$ . Note that  $\xi_{\parallel} \ll L$  in all cases. The saturation roughnesses averaged over different bilayers are in good quantitative agreement with values obtained from the refinement of XRR [21,23].

The evolution of the lateral correlation length and the saturation roughness with bilayer index provides dynamic information of the growth if the thickness increases linearly with time. Figure 2 shows the thickness (time) dependence of the saturation roughness [ $\sigma_s(t) \propto t^{\beta}$ ] and of the lateral roughness correlation length [ $\xi(t) \propto t^{1/z}$ ] for low and high-pressure samples. Very different values are obtained for the critical exponents: for high-

pressure samples  $\beta = 0.76 \pm 0.05$  and  $1/z = 0.70 \pm 0.05$ , the low-pressure samples show a saturation roughness increasing with a small exponent  $\beta = 0.25 \pm 0.05$  and an almost thickness independent correlation length. This behavior of the low-pressure samples was confirmed for samples with a larger number of bilayers (up to 40).

Interestingly,  $\log \sigma(l, t)$  is approximately linear with  $\log t$  at short time with an exponent  $\beta_{\text{loc}} = 0.25 \pm 0.05$  independent of growth conditions [Fig. 2(c)]. In the high-pressure samples, independently determined roughness exponents are in good agreement with the relation  $\alpha_{\text{loc}} = (\beta - \beta_{\text{loc}})z$  predicted by López and co-workers [9,11,12] in the case of anomalous kinetic roughening. Using  $\alpha_{\text{loc}} = \alpha - \beta_{\text{loc}}z$  the global roughness exponent  $\alpha = 1.05 \pm 0.05$ . Note that in the low-pressure samples the time exponent,  $\beta$ , of the global roughness is nearly the same as that determined from its short-range behavior  $\beta_{\text{loc}} = 0.25$ . This behavior, in which  $\beta \approx \beta_{\text{loc}}$  together with  $1/z \approx 0$ , does not allow determining the global roughness exponent.

To the best of our knowledge, the set of critical exponents obtained in our experiments do not fit in any of the existing model classes of surface growth that are known to exhibit anomalous scaling. See Table I for comparison. This shows that kinetic roughening is more complex in superlattices than in single films. An important question is the influence of this complex behavior on the results of diffuse XRR. Models to extract quantitative information in superlattices should take into account the anomalous (*non-self-affine*) roughness and the increase in the lateral roughness correlation length (nonconformal roughness).

Further insight into the mechanism of interface roughening can be obtained from the evolution of the ratio of the saturation interface width (scaling as  $t^{\beta}$ ) to the lateral roughness correlation length (scaling as  $t^{1/z}$ ). These provide a measure of the average interface slope and define the aspect ratio of the interface (inset of Fig. 3). It follows from the scaling properties outlined above that the average interface slope scales with thickness (time) as  $t^{\beta}/t^{1/z}$ . It increases slightly with thickness for the low-pressure samples [as expected from a thickness (time) independent lateral roughness correlation length], and it remains essentially constant with thickness for the high-pressure ones (Fig. 3). The time independent aspect ratio of the high-pressure samples points to a growth mechanism

TABLE I. Critical exponents determined experimentally in this work for high (8 and 10 mTorr) and low (4, 5, and 6 mTorr) pressure samples compared with exponents determined for various growth models after Ref. [11]. Here  $\alpha_{\text{loc}}$ ,  $\beta_{\text{loc}}$ ,  $\alpha$ , and  $1/z$  have been determined independently. (MBE: molecular-beam epitaxy.)

	$\alpha_{\text{loc}}$	$\beta_{\text{loc}}$	$\beta$	$\alpha$	$1/z$
High pressure	$0.75 \pm 0.05$	$0.22 \pm 0.05$	$0.76 \pm 0.05$	$1.05 \pm 0.05$	$0.70 \pm 0.05$
Low pressure	$0.65 \pm 0.05$	$0.22 \pm 0.05$	$0.25 \pm 0.05$	...	$\approx 0$
Linear MBE [8]	1	1/8	3/8	1.5	0.25
Random diffusion [9]	0.5			$> 0.5$	$< 0.5$
Nonlinear MBE [10,26]	0.73	1/11	1/3	1	0.33

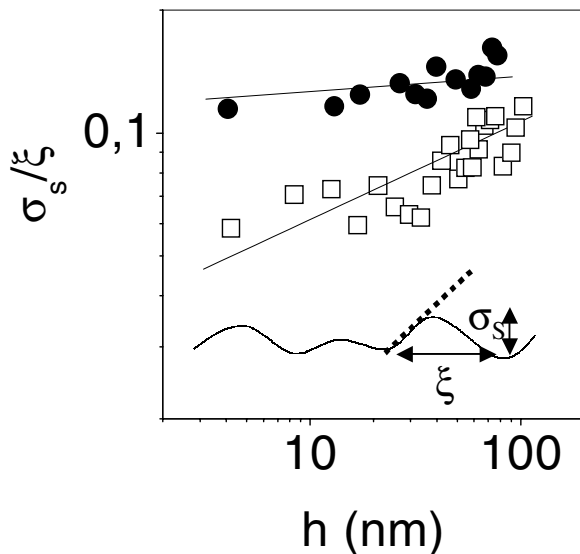


FIG. 3. Ratio of the saturation interface width to the lateral correlation length as a function of thickness (time) for 4 mTorr (open squares) and 8 mTorr samples (solid circles). This is a measure of the average long-range interface slope (see dotted line in the inset).

with a significant roughness correlation. It is interesting that changing the growth conditions results in a completely different behavior of the averaged interface slope for low and high pressures.

The scaling of the local interface slope can be obtained from the short-range local roughness, which scales as the height-height correlation function. Figure 2(c) shows that the local short-range roughness and the local interface slope show similar scaling for both kinds of samples. This may reflect that the growth processes are similar at atomic scale, but different at long scale, probably due to nonlocal (shadowing) effects [24]. The importance of long-range interactions in growth processes proposed theoretically [25] showed that the critical exponents might depend on the details of the interaction. The differences between short- and long-range behavior highlighted by the anomalous roughness may be uncovering a complicated scenario which has not been included in existing theories of surface growth.

In summary, we present imaging of the individual layers in sputtered Fe-Cr superlattices by EFTEM. A statistical analysis of the local interface width for the individual layers shows anomalous *non-self-affine* roughness characterized by a time dependent local interface width. Varying deposition conditions result in important changes in the critical exponents, from a thickness (time) independent lateral roughness correlation length at low deposition pressures to a strong increase with bilayer index at high pressures. This shows that kinetic roughening might be significantly more complicated in superlattices than in single surfaces.

J. S., J. L. V., and I. K. S. thank New del Amo Program and MEG thanks COLCIENCIAS for international

travel. DOE supported work at UCSD and at NCEM/LBL (Contract No. DE-ACO3-76SF00098). We thank Marie Claire Cyrille for work in the initial stage of this experiment and S. K. Sinha for useful conversations. J. S. thanks CICYT MAT 2000-1468 for support.

\*On leave from Universidad Complutense, Madrid, Spain.

†On leave from Universidad del Valle, Cali, Colombia.

- [1] A. L. Barabasi and H. E. Stanley, in *Fractal Concepts in Surface Growth* (Cambridge University Press, Cambridge, 1995).
- [2] D. G. Stearns, *J. Appl. Phys.* **71**, 4286 (1992); J. Villain, *J. Phys. I (France)* **1**, 19 (1991).
- [3] T. Salditt, T. H. Metzger, and J. Peisl, *Phys. Rev. Lett.* **73**, 2228 (1994).
- [4] R. Paniago *et al.*, *Phys. Rev. B* **52**, R17502 (1995).
- [5] Y. H. Phang, D. E. Savage, R. Kariotis, and M. G. Lagally, *J. Appl. Phys.* **74**, 3181 (1993).
- [6] S. K. Sinha, E. B. Sirota, S. Garoff, and H. B. Stanley, *Phys. Rev. B* **38**, 2297 (1988).
- [7] F. Family and T. Vicsek, *J. Phys. A* **18**, L75 (1985).
- [8] J. G. Amar, P.-M. Lam, and F. Family, *Phys. Rev. E* **47**, 3242 (1997); S. Das Sarma, S. V. Ghaisas, and J. M. Kim, *Phys. Rev. E* **49**, 122 (1994).
- [9] J. M. Lopez and M. A. Rodriguez, *Phys. Rev. E* **54**, R2189 (1996).
- [10] Z. W. Lai and S. Das Sarma, *Phys. Rev. Lett.* **66**, 2348 (1991); J. M. Kim and S. Das Sarma, *Phys. Rev. Lett.* **72**, 2903 (1994).
- [11] J. M. Lopez, *Phys. Rev. Lett.* **83**, 4594 (1999).
- [12] J. J. Ramasco, J. M. Lopez, and M. A. Rodriguez, *Phys. Rev. Lett.* **84**, 2199 (2000).
- [13] D. E. Wolf and J. Villain, *Europhys. Lett.* **13**, 389 (1990).
- [14] S. Das Sarma and P. Tamborenea, *Phys. Rev. Lett.* **66**, 325 (1991).
- [15] H.-N. Yang, G.-C. Wang, and T.-M. Lu, *Phys. Rev. Lett.* **73**, 2348 (1994).
- [16] J. H. Jeffries, J.-K. Zuo, and M. M. Craig, *Phys. Rev. Lett.* **76**, 4931 (1996).
- [17] S. Huo and W. Schwarzacher, *Phys. Rev. Lett.* **86**, 256 (2001).
- [18] Y.-P. Zhao *et al.*, *Phys. Rev. Lett.* **85**, 3229 (2000).
- [19] R. F. Egerton, *Electron Energy-Loss Spectroscopy in the Electron Microscope* (Plenum Press, New York, 1996).
- [20] We thank S. K. Sinha for pointing this out.
- [21] J. Santamaria *et al.*, *Phys. Rev. B* **65**, 012412 (2002).
- [22] Note that non-Gaussian distribution was used also for multilayers with terraces or nonfractal interfaces. See, e.g., V. Holy, U. Pietsch, and T. Baumbach, in *High Resolution X-ray Scattering from Thin Layers and Multilayers* (Springer, Berlin, 1999).
- [23] M. C. Cyrille *et al.*, *Phys. Rev. B* **62**, 15079 (2000).
- [24] K. Meyer, I. K. Schuller, and C. M. Falco, *J. Appl. Phys.* **52**, 5803 (1981).
- [25] S. Mukherji and S. M. Bhattacharjee, *Phys. Rev. Lett.* **79**, 2502 (1997).
- [26] S. Das Sarma *et al.*, *Phys. Rev. E* **53**, 359 (1996); C. Dasgupta, S. Das Sarma, and J. M. Kim, *Phys. Rev. E* **54**, R4552 (1996).